Enhancing security and capacity in FSO transmission for next-generation networks using OFDM/OCDMA-based ICSM codes

Somia A. Abd El-Mottaleb[1], Mehtab Singh[2], Samah Alshathri[3]*, Walid El-Shafai[4,5]* and Moustafa H. Aly [ID] [6]

[1]Alexandria Higher Institute of Engineering and Technology, Alexandria, Egypt, [2]Department of Electronics and Communication Engineering, University Institute of Engineering, Chandigarh University, Mohali, Punjab, India, [3]Department of Information Technology, College of Computer and Information Sciences, Princess Nourah bint Abdulrahman University, Riyadh, Saudi Arabia, [4]Security Engineering Laboratory, Computer Science Department, Prince Sultan University, Riyadh, Saudi Arabia, [5]Department of Electronics and Electrical Communications Engineering, Faculty of Electronic Engineering, Menoufia University, Menouf, Egypt, [6]Electronics and Communications Engineering Department, College of Engineering and Technology, Arab Academy for Science, Technology and Maritime Transport, Alexandria, Egypt

In order to address the growing demands for both enhanced security levels and increased transmission capacity, this research proposes a novel approach for free space optical (FSO) transmission. The proposed design incorporates an identity column shift matrix (ICSM) code to ensure robust security. Additionally, capacity enhancement is achieved through the utilization of a 4-level quadrature amplitude modulation (4-QAM) scheme in conjunction with an orthogonal frequency division multiplexing (OFDM) modulator. The performance of the system is evaluated across three channels, each transmitting data at a rate of 20 Gb/s, while operating in an FSO channel that is subjected to varying atmospheric attenuation effects and atmospheric turbulence. Real meteorological data from three different cities [Alexandria, Egypt; Jeddah, Kingdom of Saudi Arabia (KSA); and Hyderabad, India], situated across two continents, are incorporated to demonstrate the practicality of implementing the proposed model in real-world environments. The experimental results reveal that an increase in atmospheric turbulence leads to a higher bit error rate (BER) and lower received optical power (ROP), resulting in degraded data reception. Furthermore, the study examines the impact of weather conditions, indicating that the longest and shortest propagation ranges of 12.5 and 0.286 km, respectively, are achieved under clear weather and heavy dust storms. These conditions yield an ROP of −9.5 dBm and a log (BER) of approximately −2.5. Conversely, in the presence of strong turbulence, the performance further deteriorates. The proposed model demonstrates its ability to transmit a message signal over a distance of 0.8375 km, with a log (BER) of −2.6 under weak atmospheric turbulence. However, under strong atmospheric turbulence at the same distance, the log (BER) increases to −0.5. Regarding specific cities, the FSO range for transmitting information signals is found to be 9.58 km in Jeddah, which decreases to 6.58 km in Alexandria and 5.17 km in Hyderabad due to the increased atmospheric attenuation in these cities.

1 Introduction

The amount of mobile data traffic is increasing at an exponential rate annually, in conjunction with the rising number of mobile users across the globe. It is expected that by the end of the year 2025, there will be more than two billion individuals worldwide utilizing 5G technology. Due to this outcome, the current cellular networks will be incapable of fulfilling the traffic requirements [1].

The upcoming mobile networks will also address the evolving patterns of data traffic applications that demand high bandwidth. These applications will be a crucial aspect of the commercial drive for updated mobile solutions and enhanced networks. Moreover, essential benchmarks indicate that mobile systems beyond 5G must have the capability to accommodate a density of 10 million connections per square kilometer, handle 500 exabytes of traffic per month, and provide data rates of 1 Gb/s for a few devices and 100 Mb/s for tens of thousands of users concentrated in high-traffic locations [2].

Out of the various options for implementing mobile network front-haul technologies [3–6], free-space optic (FSO) communications have emerged as a popular choice, largely attributed to advancements in laser-based transmission methods [7]. FSO belongs to the category of optical wireless communication (OWC), wherein the information signal is conveyed through the atmosphere (channel) from the transmitting end to the receiving end, which is linked by a direct line-of-sight (LOS) link [8, 9]. It has been suggested as a solution for various new applications, like high-altitude platforms [10] and optical communications for satellites [11, 12]. Moreover, FSO can be used as an alternative to optical fibers as optical fibers have limited deployment flexibility, especially in densely populated urban areas, hilly areas, and associated high costs [13]. Figure 1 shows different areas where FSO can be implemented and various FSO applications for 5G.

The considerable attention given to FSO is primarily due to its immunity to radio interference, confidential connectivity, license-free usage, availability of optical broadband, ease of implementation, and high
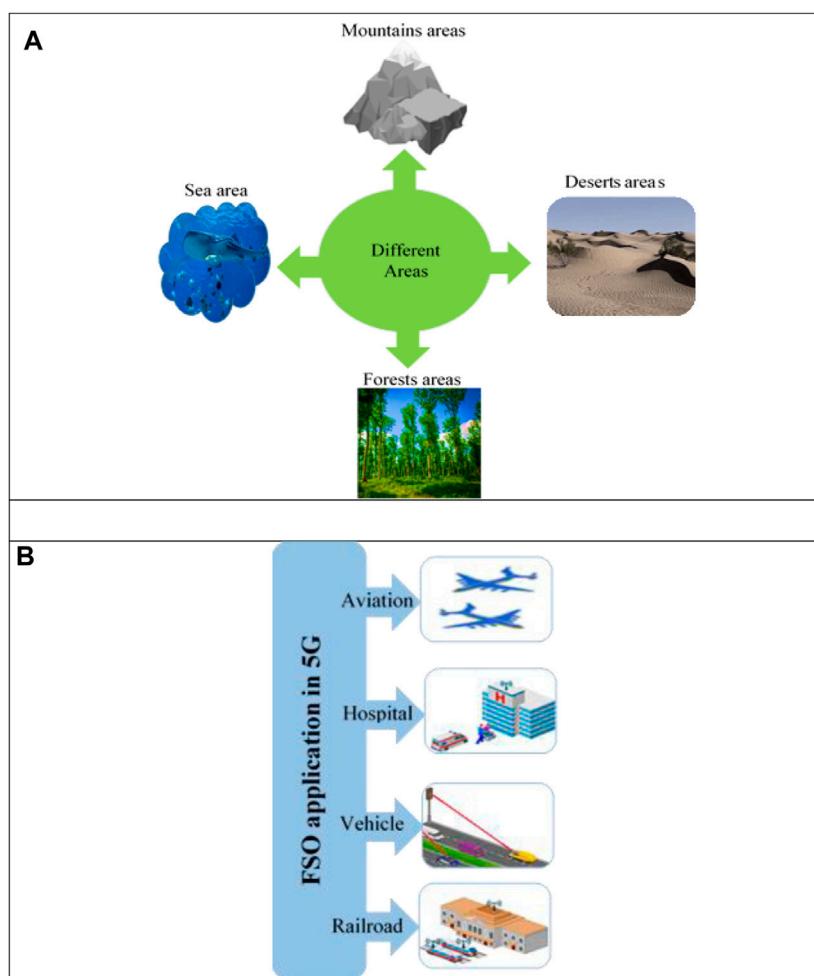

FIGURE 1
FSO **(A)** areas and **(B)** applications in 5G.

TABLE 1 Channels with their corresponding wavelengths.

Channel	λ_1 (nm)	λ_2 (nm)	λ_3 (nm)	λ_4 (nm)	λ_5 (nm)	λ_6 (nm)	λ_7 (nm)	λ_8 (nm)	λ_9 (nm)
	1,550	1,550.8	1,551.6	1,552.4	1,553.2	1,554	1,554.8	1,555.6	1,556.4
1	1	0	0	0	1	0	0	0	1
2	0	0	1	1	0	0	0	1	0
3	0	1	0	0	0	1	1	0	0

transmission speeds [14, 15]. These factors make FSO communication useful as a backup for radio frequency (RF) connections and in terrestrial transmission. Despite these advantages, FSO transmission is significantly affected by atmospheric attenuation and atmospheric turbulence. Atmospheric attenuation refers to the decrease in strength of electromagnetic signals as they propagate through the atmosphere. This phenomenon can be caused by different atmospheric particles, including dust storms, snowfall, and fog. Such particles scatter and absorb the signals, which can result in signal loss and degradation [16–18]. As for atmospheric turbulence, it is characterized by random fluctuations in air density and temperature that cause changes in the refractive index of the air, which further leads to the distortion of information signals while they travel through the atmosphere [19].

Consequently, it is important to propose an FSO model that can perform well within these effects. On the other hand, security has been of significant concern for numerous applications in communication systems. To enhance security levels, FSO enables the incorporation of spread spectrum coding techniques like OCDMA [20, 21]. OCDMA is a prospective method for transmitting data signals from multiple users asynchronously across a network with resilience [23–25]. To enhance user privacy and security, data from each individual user are assigned with a unique code, and all information from different users is multiplexed and transmitted at the same time [26].

There are codes that can be used like random diagonal (RD) [24], enhanced double weight (EDW) [25], diagonal permutation shift (DPS) [27], and dynamic cyclic shift (DCS) [28]. Although these codes can provide encryption, the existence of phase-induced intensity noise (PIIN) due to multiple access interference (MAI), which requires suitable detection techniques to illuminate it, makes using those codes complicated [25].

So, in this study, an identity column shift matrix (ICSM) code is used in OCDMA. This code has zero cross-correlation, resulting in no existence of the PIIN [29]. So, using FSO with OCDMA that uses ICSM codes will provide secure high-data transmission. To further increase the capacity of FSO communication systems, various multiplexing techniques are employed in FSO systems. These techniques include orthogonal frequency division multiplexing (OFDM) [30], polarization division multiplexing (PDM) [31], and orbital angular momentum (OAM) [32].

OFDM is a digital technology for data transmission and multi-carrier modulation that operates in wireless communications and multipath networks [33, 34]. It employs inverse fast Fourier transform (IFFT), which requires parallel data streams to be transmitted over sub-carriers that are orthogonal and have the same frequency range. OFDM provides significant advantages such as large capacity, immunity to intersymbol interference (ISI), high spectral efficiency, and inexpensive implementation [35].

1.1 Related work

Many studies have been carried out on using OCDMA codes only, OFDM only, and both OCDMA with OFDM in FSO links. In [36], a double weight zero cross-correlation (DWZCC) code was used with the OCDMA system in the FSO link. The atmospheric turbulence impacts are considered, and 25 Gb/s was obtained. Although the DWZCC code has zero cross-correlation, its long length makes its implementation difficult. In [25], the channels used were assigned with the EDW code, and the performance of the OCDMA/FSO system was investigated under clear weather, light mist, light fog, and very light fog. The capacity was not high (3 × 622 Mb/s) as broadband LED was used. As this code has unity cross-correlation, so the detection technique, which is single photodiode detection, was used to illuminate the MAI. [35] utilized OFDM in an FSO system and evaluated its performance under the influence of clear sky and fog conditions. Their proposed system achieved an overall capacity of 40 Gb/s. The researchers also utilized the actual meteorological data to examine the efficiency of their FSO system. The performance of the FSO system proposed by [37] was evaluated under the influence of rainy weather, using meteorological data from 2003 to 2013 for Dakar, the capital of Senegal. The proposed system achieved FSO ranges ranging from 1 to 3.2 km. The FSO system proposed in [30] used OFDM with OCDMA (with EDW codes) and considered clear weather, fog, and rain conditions to evaluate its performance. The system achieved a transmission capacity of 45 Gb/s.

1.2 Contribution of this paper

The main contribution can be summarized as follows:

- Proposing a high-speed FSO link for terrestrial communications that can be implemented in diverse areas having different geographical locations.
- Providing a secure FSO transmission by using the ICSM code.
- Evaluating the system performance under atmospheric attenuation and atmospheric turbulence effects.
- Confirming its suitability in different cities based on the real meteorological data.

In this study, a highly secure FSO link is proposed. For security, the ICSM codes in OCDMA systems are used and assigned to the channels using the proposed model. For capacity enhancement, OFDM is used. Severe weather conditions like fog, snow, and dust storms with their atmospheric attenuation are considered in evaluating the system's performance. Additionally, the effects of

TABLE 2 Symbols and notifications.

h_a	Weather-induced signal attenuation
$\propto_t$	Large-scale eddy number
β_t	Small-scale eddy number
$\Gamma(.)$	Gamma function
$K_{\propto_t - \beta_t}(.)$	Modified Bessel function
σ_{ry}^2	Rytov variance
d	Normalized receiver collection lens
K	Wave number
T_{FSO}	FSO range

atmospheric turbulence are also taken into account while studying the performance of the proposed system. Moreover, to be able to implement the proposed model in a real environment, the real meteorological data on Alexandria, Egypt; Jeddah, KSA; and Hyderabad, India, are used with the same practical values that are used in real FSO experiments. BER, constellation diagrams, and ROP are the evaluation parameters that are used for examining the system's performance.

The organization of the remainder of the paper is as follows. Section 2 illustrates the ICSM code construction. The FSO channel model, including atmospheric attenuation and atmospheric turbulence impacts, is described in Section 3. The layout of the proposed FSO-based OFDM/OCDM using ICSM codes is described with analytical analysis in Section 4, followed by results and discussion in Section 5. Finally, some concluding remarks and suggestions are given in Section 6.

2 ICSM code construction

The ICSM is characterized by having a number of channels, N_c, code weight, C_w, code length, C_l, and zero cross-correlation, $\lambda_c = 0$. Its code construction is based on the four following steps [29]:

First step: an identity matrix, K, with order m is defined. Here, an identity matrix of order 3 is used as follows:

$$K_3^0 = \begin{bmatrix} 1 & 0 & 0 \\ 0 & 1 & 0 \\ 0 & 0 & 1 \end{bmatrix} = \begin{bmatrix} R_3^{01} \\ R_3^{02} \\ R_3^{03} \end{bmatrix}, \quad (1)$$

where R_3^{01}, R_3^{02}, and R_3^{03} represent the first, second, and third rows in the matrix K_3^0, respectively.

Second step: left shift is performed to each row in the matrix K, with a number of times equal to (m-1) as [29]

$$\text{First shift: } K_3^1 = \begin{bmatrix} 0 & 0 & 1 \\ 1 & 0 & 0 \\ 0 & 1 & 0 \end{bmatrix} = \begin{bmatrix} R_3^{11} \\ R_3^{12} \\ R_3^{13} \end{bmatrix}$$

$$\text{Second shift: } K_3^2 = \begin{bmatrix} 0 & 1 & 0 \\ 0 & 0 & 1 \\ 1 & 0 & 0 \end{bmatrix} = \begin{bmatrix} R_3^{21} \\ R_3^{22} \\ R_3^{23} \end{bmatrix}, \quad (2)$$

where R_3^{11}, R_3^{12}, and R_3^{13} represent the first, second, and third rows in matrix K_3^1, respectively, and R_3^{21}, R_3^{22}, and R_3^{23}, represent the first, second, and third rows in matrix K_3^2, respectively.

Third step: the matrices K_3^0, K_3^1, and K_3^2 are put in the form of a row vector having size $1 \times m^2$ as [29]

$$K_3^0 = \begin{bmatrix} R_3^{01} \\ R_3^{02} \\ R_3^{03} \end{bmatrix} \leftrightarrow K_{1 \times 3}^0 = [R_3^{01}, R_3^{02}, R_3^{03}] = [1\,0\,0\,0\,1\,0\,0\,0\,1]$$

$$K_3^1 = \begin{bmatrix} R_3^{11} \\ R_3^{12} \\ R_3^{13} \end{bmatrix} \leftrightarrow K_{1 \times 3}^1 = [R_3^{11}, R_3^{12}, R_3^{13}] = [0\,0\,1\,1\,0\,0\,0\,1\,0] \quad (3)$$

$$K_3^2 = \begin{bmatrix} R_3^{21} \\ R_3^{22} \\ R_3^{23} \end{bmatrix} \leftrightarrow K_{1 \times 3}^2 = [R_3^{21}, R_3^{22}, R_3^{23}] = [0\,1\,0\,0\,0\,1\,1\,0\,0].$$

Fourth step: finally, an ICSM matrix, M_{ICSM}, with size $m \times m^2$ will be constructed as follows:

$$M_{ICSM} = \begin{bmatrix} K_{1 \times 3}^0 \\ K_{1 \times 3}^1 \\ K_{1 \times 3}^2 \end{bmatrix} = \begin{bmatrix} 1\,0\,0\,0\,1\,0\,0\,0\,1 \\ 0\,0\,1\,1\,0\,0\,0\,1\,0 \\ 0\,1\,0\,0\,0\,1\,1\,0\,0 \end{bmatrix}. \quad (4)$$

Accordingly, the relations between N_c, C_w, C_l, and m are [29] shown as follows:

$$N_c = m, C_w = m, C_l = m^2 = N_c^2 = C_w^2. \quad (5)$$

In this paper, the three channels that are assigned with the ICSM code sequences with their corresponding wavelengths are given in Table 1.

3 FSO channel model

The main factors that affect the information signal during its transmission in free-space are atmospheric attenuation and atmospheric turbulences. In this section, a brief description of these factors is given.

3.1 Atmospheric attenuation

The external climate affects the received signal. In this study, clear sky (CS), different densities of fog [low (LF), medium (MF), and heavy (HF)], various snowfall rates [wet (WS) and dry (DS)], and different levels of dust storms [light (LD), medium (MD), and heavy (HD)] are considered. In addition to the rainy weather in three different cities, Alexandria, Egypt; Jeddah, KSA; and Hyderabad, India, the CS weather condition causes low attenuation, so it has a low impact on the transmitted signal [25]. In FSO transmission, fog-induced atmospheric attenuation is a significant issue. It is composed of small water droplets that scatter light, causing it to disperse in various directions. As a result, the optical signal is weakened, leading to reduced signal quality and strength. The atmospheric attenuation caused by fog, $\propto_f$, is expressed as [17] follows:

$$\alpha_f = \frac{3.912}{b} \left(\frac{\lambda}{550nm} \right)^{-x}, \quad (6)$$
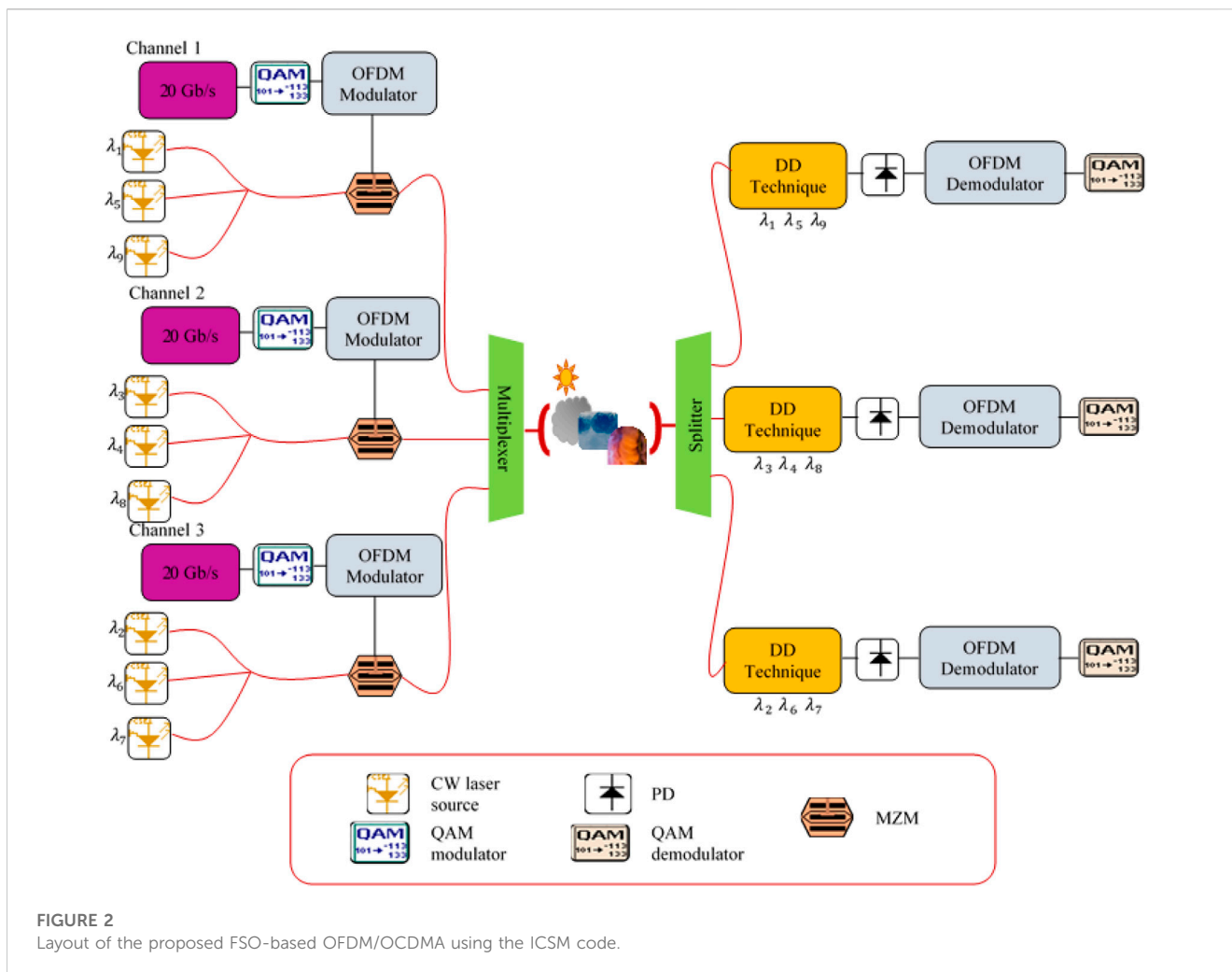
FIGURE 2
Layout of the proposed FSO-based OFDM/OCDMA using the ICSM code.

where b (km) refers to visibility and λ is the operating wavelength. The parameter x is the size distribution of the scattering particle, and its value depends on the value of b according to the Kim model (1.6 for $b > 50$; 1.3 for $6 < b < 50$; $0.16\, b + 0.34$ for $1 < b < 6$; $b − 0.5$ for $0.5 < b < 1$; 0 for $b < 0.5$) [17].

Another significant challenge in FSO communication is the snowfall-induced atmospheric attenuation [18]. It consists of ice crystals that can scatter and absorb optical signals, resulting in degradation in the received signal that carries the data. The attenuation for snow, α_s, is expressed as [18] follows:

$$\alpha_s = \begin{cases} 0.72\, R_{sf}^{\left(5.42\times10^{-5}\lambda\right)+5.49}, & \text{for WS}, \\ 1.38 R_{sf}^{\left(1.02\times10^{-4}\lambda\right)+3.78}, & \text{for DS}, \end{cases} \quad (7)$$

where R_{sf} refers to the rate of snowfall.

Moreover, dust storms pose a major challenge in the FSO transmission system due to atmospheric attenuation. This phenomenon occurs when tiny dust particles scatter and absorb optical signals, resulting in a reduction of the signal strength and quality. Its attenuation, $\propto_d$, is expressed as [32] follows:

$$\propto_d = 52 \times b^{-1.05}. \quad (8)$$

Finally, the rainy weather for 4 years from 2014 to 2018 for Alexandria, Jeddah, and Hyderabad is considered. The attenuation for rain, α_r, is expressed as [38] follows:

$$\alpha_r = 1.07\, R_{rainfall}^{0.67}, \quad (9)$$

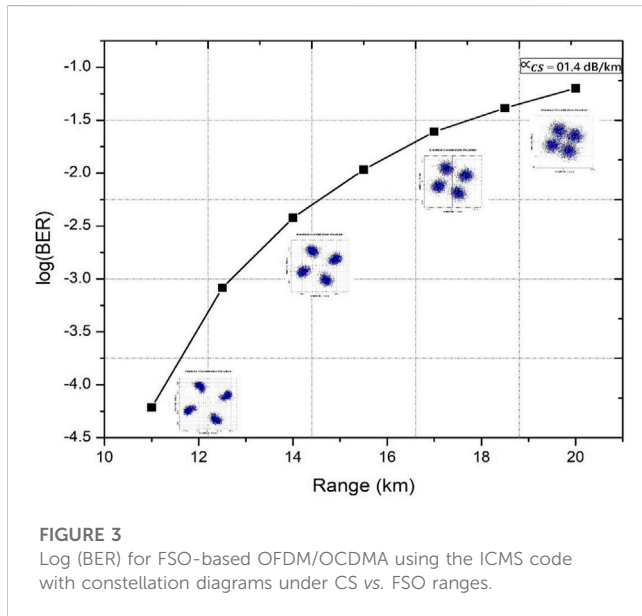where $R_{rainfall}$ refers to rainfall intensity in mm/hr.

According to www.worldweatheronline.com, accessed on 20-1-2023, the average rainfall intensities for Alexandria and Jeddah for the years 2014–2018 are 1.14 mm/h and 0.28 mm/h, respectively. Using Eq. 9, α_r will be 1.14 dB/km for Alexandria and 0.456 dB/km for Jeddah. As for Hyderabad, the average rainfall intensity and attenuation are 2.35 mm/h and 1.9 dB/km, respectively [39].

3.2 Atmospheric turbulence

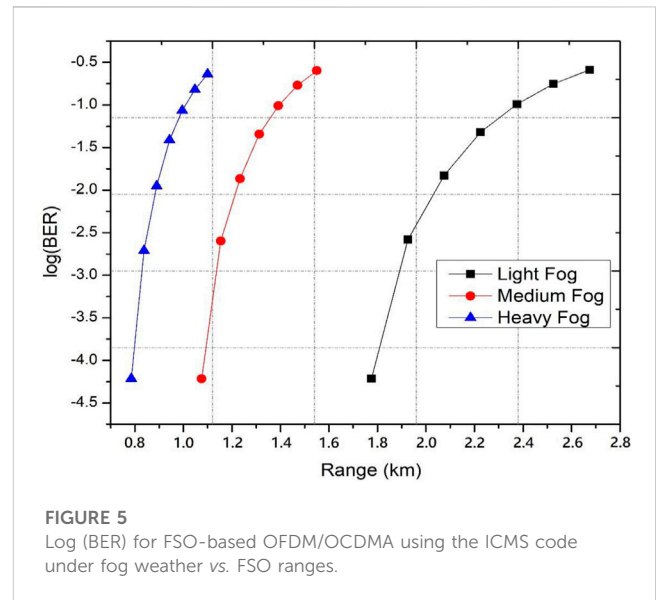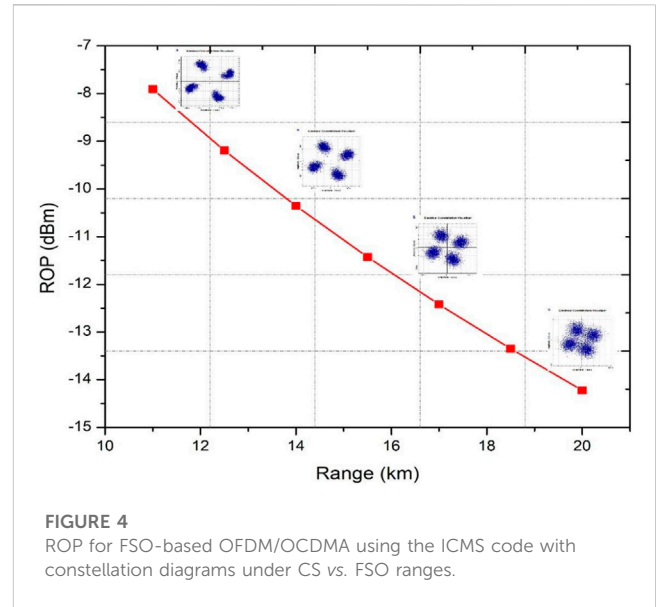Another factor that affects the signal during its propagation in free space is the atmospheric turbulence. It is characterized by random fluctuations in air density and temperature. This turbulence causes the refractive index of the air, C_n^2, to change to 1×10^{-17} m$^{-2/3}$ for weak turbulence (WT), 5×10^{-15} m$^{-2/3}$ for moderate turbulence (MT), and 1×10^{-13} m$^{-2/3}$ for strong

TABLE 3 Parameters used in simulation [18, 19, 25, 29, 38].

Parameter	Value
P_{Tra}	15 dBm
Cw	3
Cl	9
Data rate	20 Gb/s per channel
ν_e	$0.75 \times$ data rate Hz
Number of subcarriers	512
Number of FFT points	1024
Number of channels	3
Samples per bit	2
D_{Tra}	10 cm
D_{Rec}	20 cm
θ	2 mrad
$\Re$	0.8 A/W
k_B	1.38×10^{-23} J/K
T	300 K
R_L	1.03 k Ω

FIGURE 3
Log (BER) for FSO-based OFDM/OCDMA using the ICMS code with constellation diagrams under CS *vs.* FSO ranges.

FIGURE 4
ROP for FSO-based OFDM/OCDMA using the ICMS code with constellation diagrams under CS *vs.* FSO ranges.

FIGURE 5
Log (BER) for FSO-based OFDM/OCDMA using the ICMS code under fog weather *vs.* FSO ranges.

turbulence (ST), leading to a distortion in the optical signal as it travels through the atmosphere [19]. Among several models used for modeling the FSO channel when exposed to turbulence, the gamma–gamma (GG) distribution is used as it can be used for different turbulence levels [40]. The probability density function, P, of the GG distribution is given as [19] follows:
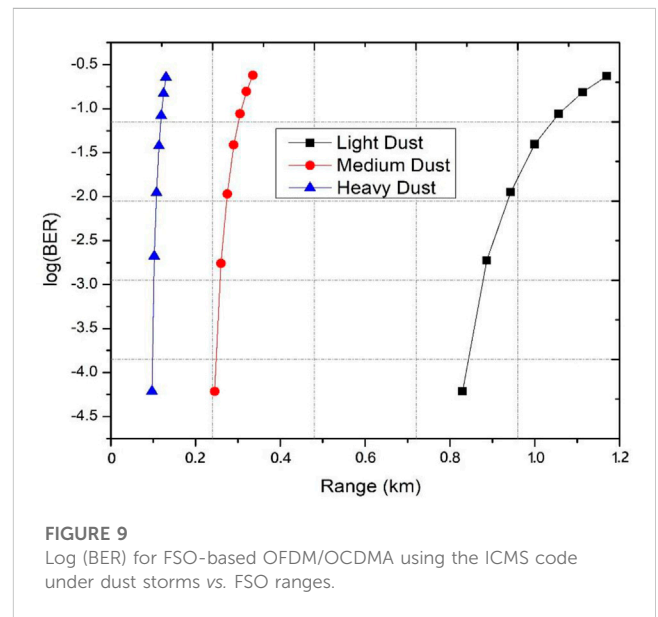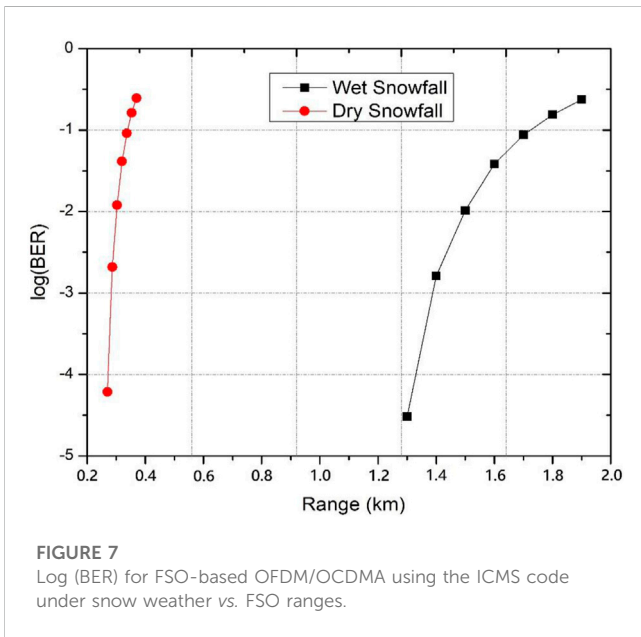
$$P(h_a) = \frac{2\left(\propto_t \beta_t\right)^{\frac{\propto_t + \beta_t}{2}}}{\Gamma(\propto_t)\Gamma(\beta_t)} h_a^{\frac{(\propto_t + \beta_t)}{2}} K_{\propto_t - \beta_t}\left(2\sqrt{\propto_t \beta_t h_a}\right); \quad h_a > 0,$$
(10)

$$\propto_t = \left\{ \exp\left[\frac{0.49\sigma_{ry}^2}{\left(1 + 0.65d^2 + 1.11\sigma_{ry}^{12/5}\right)^{7/6}}\right] - 1 \right\}^{-1},$$
(11)

$$\beta_t = \left\{ \exp\left[\frac{0.51\sigma_{ry}^2\left(1 + 0.69\sigma_{ry}^{12/5}\right)^{-5/6}}{1 + 0.9d^2 + 0.62\sigma_{ry}^{12/5}}\right] - 1 \right\}^{-1},$$
(12)

$$\sigma_{ry}^2 = 1.23 C_n^2 K^{7/6} T_{FSO}^{11/6}.$$
(13)

Table 2 shows the symbols used in Eqs 10–13 [19].

FIGURE 6
ROP for FSO-based OFDM/OCDMA using the ICMS code under fog weather *vs.* FSO ranges.

FIGURE 8
ROP for FSO-based OFDM/OCDMA using the ICMS code under snow weather *vs.* FSO ranges.

FIGURE 7
Log (BER) for FSO-based OFDM/OCDMA using the ICMS code under snow weather *vs.* FSO ranges.

FIGURE 9
Log (BER) for FSO-based OFDM/OCDMA using the ICMS code under dust storms *vs.* FSO ranges.
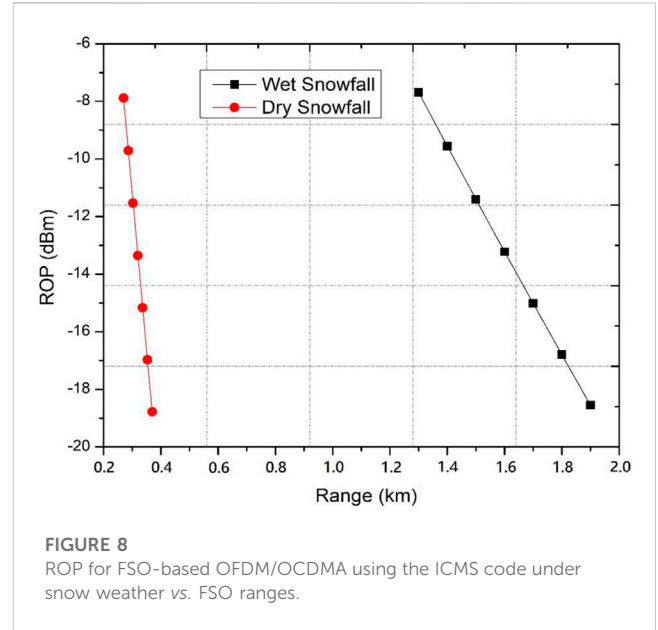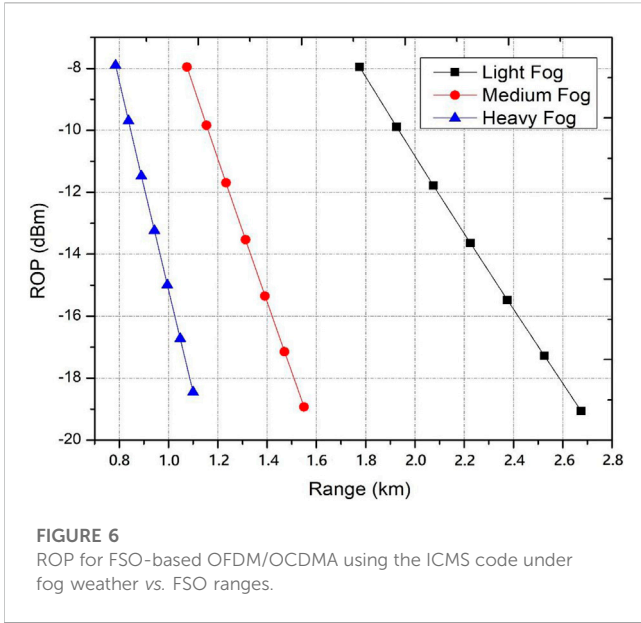
4 Proposed FSO-based OFDM/OCDMA using the ICSM code model

Figure 2 shows the setup of the proposed FSO-based OFDM/OCDMA using the ICSM model.

The transmitter processes 20 Gb/s of data through a 4-level quadrature amplitude modulation (4-QAM) sequence generator that uses 2 bits per symbol. The resulting sequence is then modulated with a 512-subcarrier-based OFDM modulator. For each channel, three light sources, which are continuous wave (CW) lasers, are used to generate the wavelengths that correspond to the ICSM code sequences, according to Table 1. To modulate the 20 Gb/s data on the light signals that are assigned to each channel, Mach–Zehnder modulators (MZMs) are used. Before being transmitted through the

FSO channel, the multiplexer (MUX) combines the light signals from the three channels. The information signal is then transferred through the FSO channel. Its received power is expressed as [25, 31] follows:

$$P_{Rec} = P_{Tra}\left(\frac{D_{Rec}}{D_{Tra} + \theta T_{FSO}}\right)^2 10^{\frac{-\propto_{at} T_{FSO}}{10}}, \qquad (14)$$

where P_{Rec} (dBm) is the received power, P_{Tra} (dBm) is the transmitted power, D_{Rec} and D_{Tra} (cm) denote the diameters of the receiver and transmitter apertures, respectively, θ (mrad) refers to the angle of the beam divergence, and $\propto_{at}$ (dB/km) indicates atmospheric attenuation.

Furthermore, the message signal is received at the receiver, which is split into three branches. Each branch uses the direct detection (DD) technique for detecting the required channel.
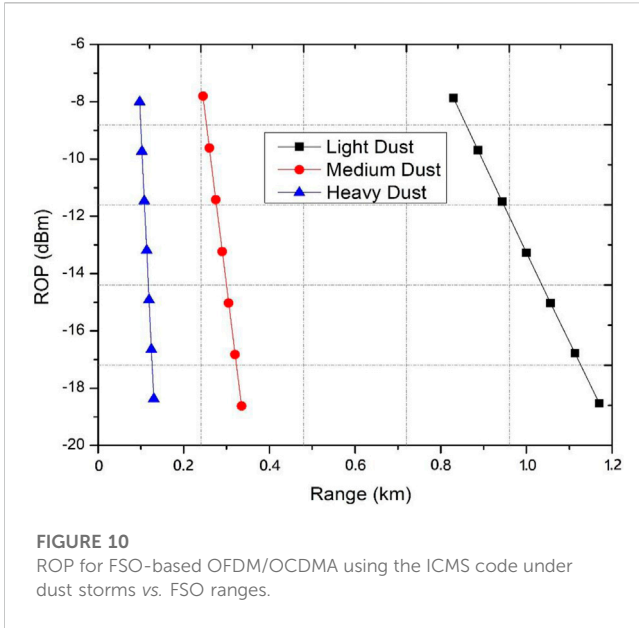
FIGURE 10
ROP for FSO-based OFDM/OCDMA using the ICMS code under dust storms *vs.* FSO ranges.

TABLE 4 Maximum propagation ranges obtained at log (BER) ~ −2.5 and ROP ~ −9.5 dBm under different weather conditions.

Weather		FSO range (km)
CS		12.5
Fog	Light	1.925
	Medium	1.154
	Heavy	0.838
Snowfall	Wet	1.4
	Dry	0.286
Dust storms	Light	0.886
	Medium	0.260
	Heavy	0.103

After detecting the signal, the photodetector (PD) is used to convert the light signal to an electrical signal. To extract the information signal, the resulting electrical signal is demodulated using an OFDM demodulator and a 4-QAM demodulator.

The output current from the PD is given as [29, 33] follows:

$$I_o = \frac{P_{RS}Cw\Re}{Cl}\sum_{n=1}^{512}Y_n e^{j2\pi f_n t}, \qquad (15)$$

where $\Re$ is the PD responsivity, Y_n is the complex data, n is the number of subcarriers, and f_n is the frequency of the nth subcarrier.

As to be sure that any two subcarriers are orthogonal, the following condition must be achieved [41]:

$$f_n = \frac{n-1}{512}. \qquad (16)$$

The shot noise, σ_{SN}^2, is expressed as [29, 41] follows:

$$\sigma_{SN}^2 = 2ev_e <I_o> = \frac{2ev_e\, P_{RS}Cw\Re}{Cl}\sum_{n=1}^{512}Y_n e^{j2\pi f_n t}, \qquad (17)$$

where e is electron charge in C and v_e (Hz) refers to the electrical bandwidth.

The thermal noise, σ_{TN}^2, is expressed as [42] follows:

$$\sigma_{TN}^2 = \frac{4k_B T v_e}{R_L}, \qquad (18)$$

where k_B, T, and R_L, respectively, are the Boltzmann constant, the load resistance of the receiver, and the absolute temperature of the receiver, respectively.

The signal-to-noise ratio (SNR) is then expressed as [36, 42] follows:

$$SNR = \frac{\left(\frac{P_{RS}Cw\Re}{Cl}\sum_{n=1}^{512}Y_n e^{j2\pi f_n t}\right)^2}{\frac{ev_e\, P_{RS}Cw\Re}{Cl}\sum_{n=1}^{512}Y_n e^{j2\pi f_n t} + \frac{4k_B T v_e}{R_L}}. \qquad (19)$$

Finally, the BER is given in terms of SNR as [36] follows:

$$BER = \frac{1}{2}erfc\left(\frac{\sqrt{SNR}}{2\sqrt{2}}\right). \qquad (20)$$

where *erfc* is the complementary error function.

The proposed model is simulated using OptiSystem software version 19 with the parameters given in Table 3.

5 Results and discussion

In this section, the performance of the FSO based on OFDM/OCDMA using the ICMS code is investigated in three parts. The first part shows the impact of atmospheric attenuation caused by various weather changes (CS, fog, snow, and dust). The effects of different turbulences are displayed and discussed in the second part. The third part devotes the results for the suggested system performance for the three mentioned cities located in different countries having different climates according to their geographical location.

5.1 Impact of atmospheric attenuation

Figure 3 shows the effect of different transferring distances in the free space for the information signal on the proposed system performance under CS in terms of BER. It also shows the constellation at 11 km, 14 km, 17 km, and 20 km FSO ranges. It is clear that as long as the transmission distance in free space increases, log (BER) increases. At $\propto_{CS}$ = 01.4 dB/km, it allows the message signal to be propagated over a long range of 12.5 km with log (BER) < −2.5 and a good constellation of the received signal. As the threshold value of BER is = 3.8×10^{-3} [43], so the information signal is received with a worse constellation diagram at the 20-km FSO link because it has a log (BER) value of −1.19.

The effect of different transferred ranges in the free space on the ROP for the proposed system is shown in Figure 4 with constellation diagrams at FSO ranges of 11 km, 14 km, 17 km, and 20 km. It is noticed that the power of the received signal for longer FSO ranges is lower than that for shorter ranges. As shown in Figure 3, the maximum free-space transmission range is 12.5 km. So, from

TABLE 5 Summary of log (BER) at the FSO link of 0.8375 km for the proposed model under the impacts of different atmospheric turbulence.

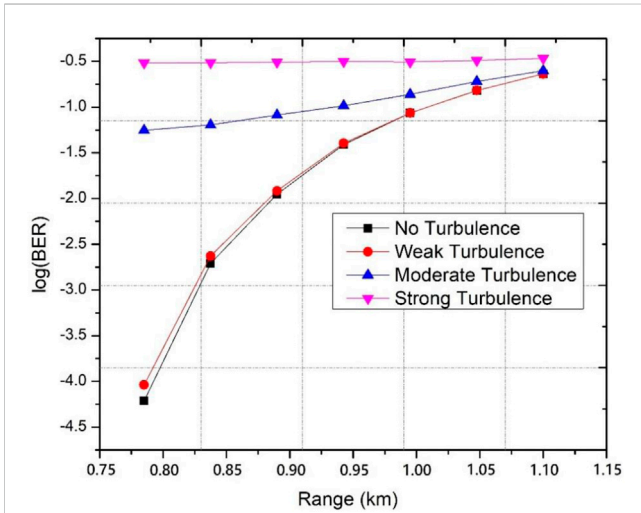| Table 5 log (BER) at the 0.8375 km transmission propagation range under different atmospheric turbulence	
Effect of turbulence	Log (BER)
Absent	−2.71
Weak	−2.62
Moderate	−1.19
Strong	−0.51

FIGURE 11
Log (BER) for FSO-based OFDM/OCDMA using the ICMS code under the impact of different atmospheric turbulence.
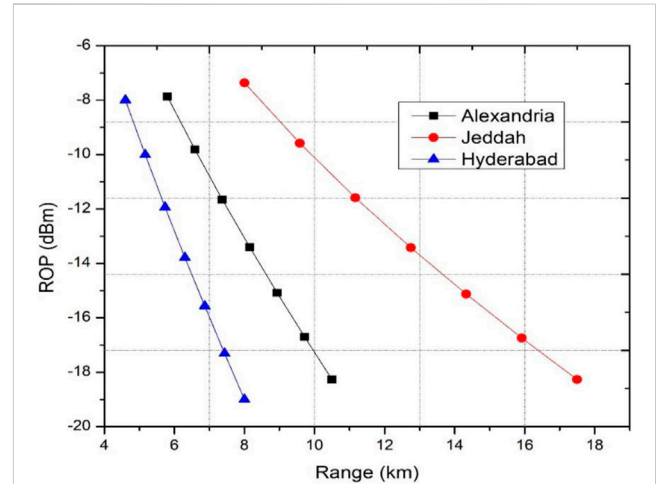

FIGURE 13
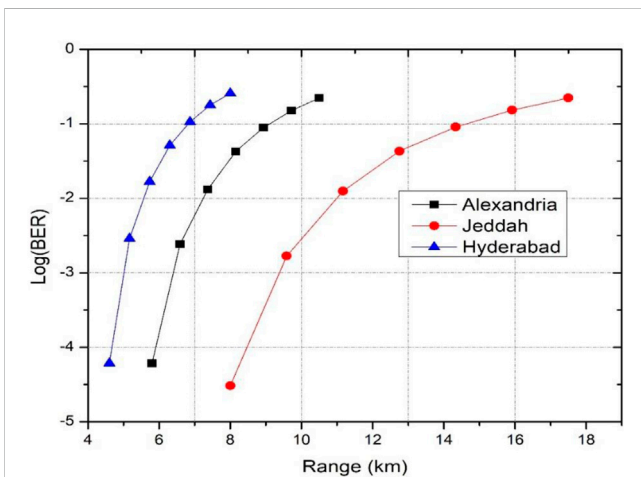ROP for FSO-based OFDM/OCDMA using the ICMS code for the three mentioned cities.

FIGURE 12
Log (BER) for FSO-based OFDM/OCDMA using the ICMS code for the three mentioned cities.

TABLE 6 Maximum propagation ranges obtained for different cities at log (BER) ~ −2.5 and an overall capacity of 60 Gb/s.

City	FSO range (km)	ROP (dBm)
Alexandria	6.58	−9.81
Jeddah	9.58	−9.58
Hyderabad	5.16	−10.01

When the atmospheric phenomenon known as fog occurs, it affects the visibility between the source, which is located at the transmitter side, and the destination, which is at the receiver side. Moreover, it degrades the ROP for the information signal as it causes attenuation, which varies from 9 dB/km to 22 dB/km according to its level of occurrence [17]. Figures 5, 6 depict the results of the log (BER) and ROP, respectively, for one channel of the proposed system under various fog conditions at different transmission distances. Low levels of fog can make the information signal travel a longer range with high ROP and low log (BER) while achieving a shorter FSO range when a heavier level of fog occurs. The maximum FSO span of 1.925 km is achieved when a low degree of fog occurs with log(BER) and ROP values of approximately −2.5 and −9.7 dBm, respectively. However, the

Figure 4, the optimum ROP that corresponds to this range is −9.19 dBm. In addition, for higher ranges, 18.5 km and 20 km, the ROP is −13.35 dBm, and −14.22 dBm, respectively.

TABLE 7 Comparison between the present study and previous studies.

	Reference [25]	Reference [30]	Reference [36]	Present work
Technique	OCDMA using the EDW code	OFDM/OCDMA using the EDW code	OCDMA using the DWZCC code	OFDM/OCDMA using the ICSM code
Turbulence effects	NA	NA	Weak, moderate, and strong	Weak, moderate, and strong
Weather conditions (transmission range)	CS (3 km), light mist (3 km), very LF (2 km), and LF (0.5 km)	CS (3.45 km), LR (1.316 km), MR (1.045 km), HR (0.7 km), LH (2.391 km), MH (1.591 km), HH (1.025 km), LF (1.085 km), MF (0.784 km), and HF (0.645 km)	NA	CS (12.5 km), LF (1.925 km), MF (1.154 km), HF (0.838 km), WS (1.4 km), DS (0.286 km), LD (0.886 km), MD (0.260 km), and HD (0.103 km)
Data rate	3 × 622 Mb/s	3 × 15 Gb/s	10 × 2.5 Gb/s	3 × 20 Gb/s
Real meteorological data	NA	NA	NA	Alexandria, Jeddah, and Hyderabad

transmission free-space distance achieved at nearly the same log (BER) and ROP values when there is medium fog is 1.154 km, which is shorter than that achieved under LF as MF has $\propto_f$ greater than LF. The minimum FSO link of 0.8375 km, as expected, is obtained when there is a heavy level of fog as HF has the larger value for $\propto_f$.

Moreover, the performance of the proposed FSO-based OFDM/OCDMA using the ICSM code is investigated under the impact of different snowfalls (WS or DS). The effect of different free-space transmission ranges with respect to log (BER) and ROP of the received signal is evaluated and plotted in Figures 7, 8, respectively. As the attenuation of WS and DS is 13.73 dB/km and 96.8 dB/km [18], respectively, so the information signal will propagate under their effects in free space a distance shorter than that achieved when fog occurs. For WS, the maximum propagation range is 1.4 km with an ROP of −9.55 dBm, which is decreased to 0.286 km with the same value of ROP when the snowfall becomes dry. These values are within the acceptable log (BER) value (below −2.5).

Furthermore, the severe event of a dust storm has a negative effect on the information signal-received power causing high BER. This is because the values of $\propto_d$ according to the strength of the dust storm are larger than those of $\propto_f$ and $\propto_s$. Its values vary as for LD, $\propto_d = 25.11$ dB/km, while for MD and HD, the values of $\propto_d$ are 107.11 dB/km and 297.38 dB/km, respectively [32]. Figures 9, 10 demonstrate log (BER) and ROP, respectively, vs. different FSO spans. Comparing Figure 9 with Figures 5, 7, it is noticed that the shortest distances achieved by the information signal are under various dust storms. These free-space distances are 0.886 km under LD, 0.260 km under MD, and 0.102 km under HD with log (BER) below −2.6. At these ranges, the ROP is −9.7 dBm.

Tables 4, 5 summarize the maximum free-space distances that are obtained under different climate changes at a log (BER) value of ~ −2.5 and ROP of ~ −9.5 dBm at 60 Gb/s overall capacity.

5.2 Impact of atmospheric turbulences

In this section, the impact of different atmospheric turbulence on the proposed system performance is given. Figure 11 shows log (BER) vs. different free-space transmission distances for different atmospheric turbulence effects. One can notice that in case of no

turbulence and WT, the signal can travel up to 0.8375 km with log (BER) equal −2.7, while for MT and HT, as the refractive index of air increases, the performance degrades, achieving log (BER) −1.19 and −0.5 under MT and ST.

For the FSO channel in OptiSystem ver. 20, we selected the gamma–gamma model and changed the value of C_n^2 according to the turbulence effect (weak, moderate, and strong). The value of C_n^2 is set as 5×10^{-13}, 5×10^{-15}, and 5×10^{-17} $m^{-2/3}$ for strong, moderate, and weak turbulence, respectively.

5.3 Impact of rainy weather in the cities of Alexandria, Jeddah, and Hyderabad

Finally, to show the availability of implementing the proposed FSO-based OFDM/OCDMA using the ICSM code, the performance is studied based on real meteorological data for three different cities located in two different continents (Africa and Asia). Figure 12 shows the performance in terms of log (BER) against FSO spans for different cities. As α_r in Jeddah is lower than that in Alexandria and Hyderabad, so the longest free-space transmission distance of 9.58 km is obtained in Jeddah, which is decreased to 6.58 km and 5.17 km in Alexandria and Hyderabad, respectively. This is expected as Hyderabad has the lowest value of α_r. These ranges are obtained at log (BER) ~ −2.5.

Additionally, the ROP performance is investigated and plotted in Figure 13 for these cities. The value of ROP degrades while the FSO span increases. Comparing propagation ranges in Figure 13 with Figure 12, the ROPs corresponding to 9.58 km in Jeddah, 6.58 km in Alexandria, and 5.17 km in Hyderabad are −9.81 dB m, −9.58 dBm, and −10.01 dBm, respectively.

Table 6 summarizes the maximum free-space distances with their ROP obtained for different cities at a log (BER) value of ~ −2.5 and 60 Gb/s overall capacity.

Table 7 provides a comparison between our proposed system and previously published works, indicating the advantages of our system in terms of transmission range and data rate.

6 Conclusion

In this study, a high-speed, secure FSO transmission system is proposed to be used in 5G and beyond networks. This model is

based on using the ICSM code for security and OFDM for capacity improvement. Information data of 20 Gb/s are modulated by the OFDM modulator and transmitted on a secure ICSM code. As three channels are used, so a total capacity of 60 Gb/s is conducted. Moreover, atmospheric attenuation that results from fog, snow, and dust weather and atmospheric turbulence that occurs due to changes in air temperature are considered. Furthermore, the actual meteorological data regarding the average rainfall intensities in Alexandria, Jeddah, and Hyderabad are incorporated to validate and evaluate the performance of our proposed FSO-based OFDM/OCDMA using the ICSM code model in a practical scenario.

The effects of various conditions on the FSO system performance are evaluated by measuring log (BER), constellation diagrams, and assessing ROP. The obtained results show that as $\propto$ increases, information signals are transferred short distances, log (BER) increases, and consequently, the performance becomes worse, and ROP degrades. The longest free-space span is achieved under CS of 12.5 km, while the shortest is obtained under an HD of 0.103 km with a log (BER) value of ~ −2.5 and ROP of ~-9.5 dBm. Additionally, the presence of ST has a negative impact on the received signal compared to WT. Due to the higher value of C_n^2, when ST occurs, the performance is worst under its effect. At an FSO range of 0.8375 km, log (BER) increases from −2.6 to −0.5 when atmospheric turbulence varies from WT to ST. So, the information will not be received under the effect of ST. Moreover, with the proposed model, in Alexandria, Jeddah, and Hyderabad, the maximum achieved FSO span with ROP obtained corresponding to these cities is 6.58 km and −9.58 dBm, 9.58 km and −9.81 dBm, and 5.17 km and −10.01 dBm, respectively. Consequently, our suggested model is recommended to be used in 5G beyond networks and applications.

Data availability statement

The original contributions presented in the study are included in the article/Supplementary Material. Further inquiries can be directed to the corresponding author.

Author contributions

All authors listed have made a substantial, direct, and intellectual contribution to the work and approved it for publication.

Conflict of interest

The authors declare that the research was conducted in the absence of any commercial or financial relationships that could be construed as a potential conflict of interest.

Publisher's note

All claims expressed in this article are solely those of the authors and do not necessarily represent those of their affiliated organizations, or those of the publisher, the editors, and the reviewers. Any product that may be evaluated in this article, or claim that may be made by its manufacturer, is not guaranteed or endorsed by the publisher.

References

1. Carson S, Davies S. A pressure release valve: South Korean long-term care policy as supplemental to family elder care. *Ericsson Mobility Rep November* (2022) 1–24. doi:10.1080/08959420.2022.2133318

2. Raddo TR, Rommel S, Cimoli B, Vagionas C, Perez-Galacho D, Pikasis E, et al. Transition technologies towards 6G networks. *EURASIP J Wirel Commun Netw* (2021) 100:100–22. doi:10.1186/s13638-021-01973-9

3. Ishimura S, Takahashi H, Inohara R, Nishimura K, Tsuritani T, Suzuki M. High-capacity and high-fidelity analog radioover-fiber mobile fronthaul. In: Proceedings of the Metro and Data Center Optic Networks and Short-Reach Links V; San Francisco, CA, USA, 12027 (2022). 119–22.

4. Alzenad M, Shakir MZ, Yanikomeroglu H, Alouini M–S. FSO-based vertical backhaul/fronthaul framework for 5G+ wireless networks. *IEEE Commun Mag* (2018) 56:218–24. doi:10.1109/mcom.2017.1600735

5. Mukhopadhyay A, Ruffini M. Design methodology for wireless backhaul/fronthaul using free space optics and fibers. *J Light Technol* (2023) 41:17–30. doi:10.1109/jlt.2022.3210524

6. Gu Z, Zhang J, Sun X, Ji Y. Optimizing networked flying platform deployment and access point association in FSO-based fronthaul networks. *IEEE Wirel Commun Lett* (2020) 9:1221–5. doi:10.1109/lwc.2020.2986406

7. Ishimura S, Morita R, Inoue T, Nishimura K, Takahashi H, Tsuritani T, et al. Proposal and demonstration of free-space optical communication using lens-free photonic-crystal surface-emitting laser. In: Proceedings of the European Conference on Optical Communication (ECOC) 2022; 18–22 September 2022; Basel, Switzerland (2022). paper Th3A.7.

8. Aveta F, Refai HH, Lopresti PG. Cognitive multi-point free space optical communication: Real-time users discovery using unsupervised machine learning. *IEEE Access* (2020) 8:207 575–88. doi:10.1109/access.2020.3038624

9. Shanmuga sundar D, Sathyadevaki R, Sridarshini T, Sivanantha Raja A. Photonic crystal based routers for photonic integrated on chip networks: A brief analysis. *Opt Quant Electron* (2018) 50:383. article 383. doi:10.1007/s11082-018-1655-1

10. Ata Y, Alouini M–S. HAPS based FSO links performance analysis and improvement with adaptive optics correction. In: IEEE Trans. Wirel. Commun; 27 December 2022. IEEE (2022). Early Access.

11. Samy R, Yang H–C, Rakia T, Alouini M–S. Space-air-ground FSO networks for high-throughput satellite communications. *IEEE Commun Mag* (2022) 60:82–7. doi:10.1109/mcom.002.2200018

12. Matuz B, Zahr A, Sauter A. Coherent communications for free space optical low-earth orbit downlinks. In: Proceedings of the 2022 IEEE Global Communications Conference; 4–8 December 2022; Rio de Janeiro, Brazil. GLOBECOM (2022). p. 5911–6.

13. Bekkali A, Fujita H, Hattori M. Free-space optical communication systems for B5G/6G networks. In: Proceedings of the 26th Optoelectronics and Communications Conference; 3–7 July 2021; Hong Kong, China (2021). W1A.1.

14. Garrido-Balsells JM, Javier Lopez-Martinez F, Castillo-Vázquez M, Jurado-Navas A, Puerta-Notario A. Performance analysis of FSO communications under LOS blockage. *Opt Express* (2017) 25:25278–94. doi:10.1364/oe.25.025278

15. Zhou Z, Zhang H, Chun L, Sharma A. Performance analysis of duobinary and CSRZ modulation based polarization interleaving for high-speed WDM-FSO transmission system. *J Opt Commun* (2022) 43(1):147–52. doi:10.1515/joc-2018-0188

16. Malik A, Singh P. Comparative analysis of point to point FSO system under clear and haze weather conditions. *Wirel Pers Commun* (2014) 80(2):483–92. doi:10.1007/s11277-014-2022-6

17. Kim II, McArthur B, Korevaar EJ, "Comparison of laser beam propagation at 785 nm and 1550 nm in fog and haze for optical wireless communications," in *Optical wireless communications III*, Korevaar EJ, Ed., vol. 4214, International Society for Optics and Photonics. SPIE, 26 – 37. 2001.

18. Nadeem F, Leitgeb E, Awan MS. Comparing the snow effects on hybrid network using optical wireless and GHz links. In: proceeding 2009 International Workshop on Satellite and Space Communications Tuscany; 9-11 September 2009; Siena, Italy. IEEE (2009). 171–5. doi:10.1109/IWSSC.2009.5286388

19. Vetelino FS, Young C, Andrews L, Recolons J. Aperture averaging effects on the probability density of irradiance fluctuations in moderate-to-strong turbulence. *Appl Opt* (2007) 46:2099–108. doi:10.1364/ao.46.002099

20. Jurado-Navas A, Raddo TR, Garrido-Balsells JM, Borges B–HV, Olmos JJV, Monroy IT. Hybrid optical CDMA-FSO communications network under spatially correlated gamma-gamma scintillation. *Opt Express* (2016) 24:16799–814. doi:10.1364/oe.24.016799

21. Raddo TR, Perez-Santacruz J, Johannsen U, Dayoub I, Haxha S, Monroy IT, et al. FSO-CDMA systems supporting end-to-end network slicing. In: Proceedings of the Imaging and Applied Optics Congress; 22–26 June 2020; Washington, DC, USA (2020). paper JW2A.38.

22. Raddo TR, Sanches AL, dos Reis JV, Borges B–HV. Influence of the MAI distribution over the BER evaluation in a multirate, multiclass OOC-OCDMA system. In: Proceedings of the Advanced Photonics; 12–14 June 2011; Toronto, ON, Canada (2011). paper ATuB5.

23. Mostafa S, Mohamed AE-NA, El-Samie FEA, Rashed ANZ. Performance evaluation of SAC-OCDMA system in free space optics and optical fiber system based on different types of codes. *Wirel Pers Commun* (2017) 96(2):2843–61. doi:10.1007/s11277-017-4327-8

24. Fadhil HA, Aljunid SA, Ahmad R. Performance of random diagonal code for OCDMA systems using new spectral direct detection technique. *Optic Fiber Technol* (2009) 15(3):283–9. doi:10.1016/j.yofte.2008.12.005

25. Abd El-Mottaleb SA, Métwalli A, Hassib M, Alfikky AA, Fayed HA, Aly MH. SAC-OCDMA-FSO communication system under different weather conditions: Performance enhancement. *Quant Electron* (2021) 53(11):616–33. doi:10.1007/s11082-021-03269-0

26. Upadhyay KK, Srivastava S, Shukla NK, Chaudhary S. High-speed 120 Gbps AMI-WDM-PDM free space optical transmission system. *J Opt Commun* (2019) 40:429–33. doi:10.1515/joc-2017-0086

27. Ahmed HY, Zeghid M, Bouallegue B, Chehri A, Abd El-Mottaleb SA. Reduction of complexity design of sac ocdma systems by utilizing diagonal permutation shift (DPS) codes with single photodiode (SPD) detection technique. *Electronics* (2022) 11:1224–40. doi:10.3390/electronics11081224

28. Abd TH, Aljunid SA, Fadhil HA, Ahmad RB. A new algorithm for development of dynamic cyclic shift code for spectral amplitude coding optical code division multiple access systems. *Fiber Integr Opt* (2012) 31:397–416. doi:10.1080/01468030.2012.733905

29. Alayedi M, Cherifi A, Hamida AF, Matem R, El-Mottaleb SAA. Performance improvement of SAC-OCDMA network utilizing an identity Column shifting matrix (ICSM) code. In: Abd El-Latif AA, Maleh Y, Mazurczyk W, ELAffendi M, Alkanhal IM, editors. *Advances in cybersecurity, cybercrimes, and smart emerging technologies. CCSET 2022. Engineering cyber-physical systems and critical infrastructures*, 4. Cham: Springer (2023).

30. Singh M, Riz JK, Kamruzzaman MM, Dhasarathan V, Sharma A, Abd El-Mottaleb SA. Design of a high-speed-OFDM-SAC-OCDMA-based FSO system using EDW codes for supporting 5G data services and smart city applications. *Fron Phys* (2022) 10. article 934848. doi:10.3389/fphy.2022.934848

31. Chaudhary S, Sharma A, Tang X, Wei X, Sood P. A cost effective 100 Gbps FSO system under the impact of fog by incorporating OCDMA-PDM scheme. *Wirel Pers Commun* (2020) 116:2159–68. doi:10.1007/s11277-020-07784-3

32. Singh M, Atieh A, Grover A, Barukab O. Performance analysis of 40 Gb/s free space optics transmission based on orbital angular momentum multiplexed beams. *Alexandria Eng J* (2022) 61:5203–12. doi:10.1016/j.aej.2021.10.043

33. Aldhaibani AO, Rahman TA, Aljunid SA, Hindia MN, Hanafi EB. A new model to enhance the QoS of spectral amplitude coding-optical code division multiple access system with OFDM technique. *Optic Quant Electron* (2016) 48(10):481–92. doi:10.1007/s11082-016-0750-4

34. Armstrong J. OFDM for optical communications. *J Light Technol* (2009) 27:189–204. doi:10.1109/jlt.2008.2010061

35. Li C, Yang Q. Optical OFDM/OQAM for the future fiber optics communications. *Proced Eng* (2016) 140:99–106. doi:10.1016/j.proeng.2015.09.238

36. Moghaddasi M, Seyedzadeh S, Glesk I, Lakshminarayana G, Anas SBA. DW-ZCC code based on SAC–OCDMA deploying multi-wavelength laser source for wireless optical networks. *Opt Quant Electron* (2017) 49:393. article 393. doi:10.1007/s11082-017-1217-y

37. Bamba Dath CA, Niane A, Mbaye M, Boye Faye NA. Wireless optical signal availability and link range analyses over strong fluctuating meteorological conditions with case study in Senegal. *Indian J Sci Technol* (2017) 10:1–11. doi:10.17485/ijst/2017/v10i45/110582

38. Muhammad SS, Kohldorfer P, Leitgeb E. Channel modeling for terrestrial free space optical links. In: Proc. of 2005 7th International Conference Transparent Optical Networks; 7-7July 2005; Barcelona, Spain, 1 (2005). 407–10.

39. Singh H, Mittal N, Singh H. Evaluating the performance of free space optical communication (FSOC) system under tropical weather conditions in India. *Int J Commun Syst* (2022) 35. article e5347. doi:10.1002/dac.5347

40. Feng J, Zhao X. Performance analysis of OOk-based FSO systems in gamma-gamma turbulence with imprecise channel models. *Opt Commun* (2017) 402:340–8. doi:10.1016/j.optcom.2017.06.016

41. Shieh W, Djordjevic I. *OFDM for optical communications*. London: Academic Press (2009).

42. Kaur G, Singh G. Performance analysis of SAC-OCDMA in free space optical medium using MD and DDW code. In: Proc. 2015 2nd International Conference on Recent Advances in Engineering & Computational Sciences; 21-22 Dec 2015; Chandigarh, India. RAECS (2015). 1–6.

43. Raza A, Iqbal S, Iqbal M, Mirza J, Ghafoor S, Attieh A. 400 Gbps/λ PAM-4 data transmission over FSO link by employing space division multiplexing for data center interconnects using LG modes enabled VCSELs. *Opt Quant Electron* (2023) 55:283. article no. 283. doi:10.1007/s11082-023-04572-8